



# Local Injection of Hydroxyapatite Electret Ameliorated Infarct Size After Myocardial Infarction

Junji Yamaguchi, MD; Risako Chiba; Hiroaki Komuro, PhD;  
Kensuke Ihara, MD, PhD; Kosuke Nozaki, PhD; Akiko Nagai, MD, PhD;  
Tetsushi Furukawa, MD, PhD; Tetsuo Sasano, MD, PhD

**Background:** Previous studies showed that hydroxyapatite electret (HAE) accelerates the regeneration of vascular endothelial cells and angiogenesis. This study investigated the effects of HAE in myocardial infarction (MI) model mice.

**Methods and Results:** MI was induced in mice by ligating the left anterior descending artery. Immediately after ligation, HAE, non-polarized hydroxyapatite (HAN), or water (control) was injected into the infarct border myocardium. Functional and histological analyses were performed 2 weeks later. Echocardiography revealed that HAE injection preserved left ventricular systolic function and the wall thickness of the scar, whereas HAN-injected mice had impaired cardiac function and thinning of the wall, similar to control mice. Histological assessment showed that HAE injection significantly attenuated the length of the scar lesion. There was significant accumulation of CD31-positive cells and increased expression of vascular endothelial growth factor (*Vegf*), intercellular adhesion molecule-1 (*Icam1*), vascular cell adhesion molecule-1 (*Vcam1*), hypoxia-inducible factor-1 $\alpha$  (*Hif1a*), and C-X-C motif chemokine ligand 12 (*Cxcl12*) genes in the infarct border zone of HAE-injected mice. These effects were not induced by HAN injection. Anti-VEGFR2 antibody canceled the beneficial effect of HAE. In vitro experiments in a human cardiovascular endothelial cell line showed that HAE dose-dependently increased *VEGFA* expression.

**Conclusions:** Local injection of HAE attenuated infarct size and improved cardiac function after MI, probably due to angiogenesis. The electric charge of HAE may stimulate angiogenesis via HIF1 $\alpha$ -CXCL12/VEGF signaling.

**Key Words:** Angiogenesis; Hydroxyapatite electret; Myocardial infarction; Ventricular remodeling

Myocardial infarction (MI) is the leading cause of morbidity and mortality in developed countries. MI is caused by the occlusion of a coronary artery, followed by necrosis of the infarct area and resulting in impaired cardiac function. Recent progress in emergency care and patient management has improved the prognosis of patients with acute MI.<sup>1</sup> However, a substantial number of patients develop heart failure because of a persistent reduction in cardiac function.

Hydroxyapatite (HA; Ca<sub>10</sub>(PO<sub>4</sub>)<sub>6</sub>(OH)<sub>2</sub>) is one of the most frequently used biomaterials to form bones and teeth.<sup>2</sup> It is known as one of the most biocompatible agents. HA is electrically neutral in its original form, but the application of heat and pressure to HA generates durably polarized HA, called hydroxyapatite electret (HAE).<sup>3</sup> Similar to non-polarized HA (HAN), HAE induces the adsorption of proteins, such as fibrin and blood coagulation factors.<sup>4,5</sup>

Furthermore, previous studies showed the ability of HAE to stimulate bone formation accompanied by angiogenesis, and to accelerate the regeneration of endothelial cells.<sup>6,7</sup> Based on these findings, we hypothesized that HAE may have favorable effects in the treatment of MI. Thus, the aim of the present study was to examine the effects of local injections of HAE into the infarct border zone in a murine model of anterior MI.

## Methods

### Preparation and Characterization of HAE

HA was synthesized by a wet method, as described previously.<sup>8</sup> Macro- and microscopic images of HA are shown in **Figure 1A,B**. The crystal phase of the specimen was analyzed using powder X-ray diffraction (XRD; Bruker AXS D8 Advance; Bruker, Billerica, MA, USA) and Cu

Received July 16, 2021; revised manuscript received November 1, 2021; accepted November 4, 2021; J-STAGE Advance Publication released online December 1, 2021 Time for primary review: 15 days

Department of Cardiovascular Medicine (J.Y., T.S.), Department of Cardiovascular Physiology (R.C., H.K.), Department of Bio-informational Pharmacology, Medical Research Institute (K.I., T.F.), Tokyo Medical and Dental University, Tokyo; Department of Fixed Prosthodontics, Graduate School of Medical and Dental Sciences, Tokyo Medical and Dental University, Tokyo (K.N.); and Department of Anatomy, Aichi-Gakuin University School of Dentistry, Nagoya (A.N.), Japan

Mailing address: Tetsuo Sasano, MD, PhD, Department of Cardiovascular Medicine, Tokyo Medical and Dental University Hospital, 1-5-45 Yushima, Bunkyo-ku, Tokyo 113-8510, Japan. E-mail: sasano.cvm@tmd.ac.jp

All rights are reserved to the Japanese Circulation Society. For permissions, please e-mail: cr@j-circ.or.jp

ISSN-2434-0790



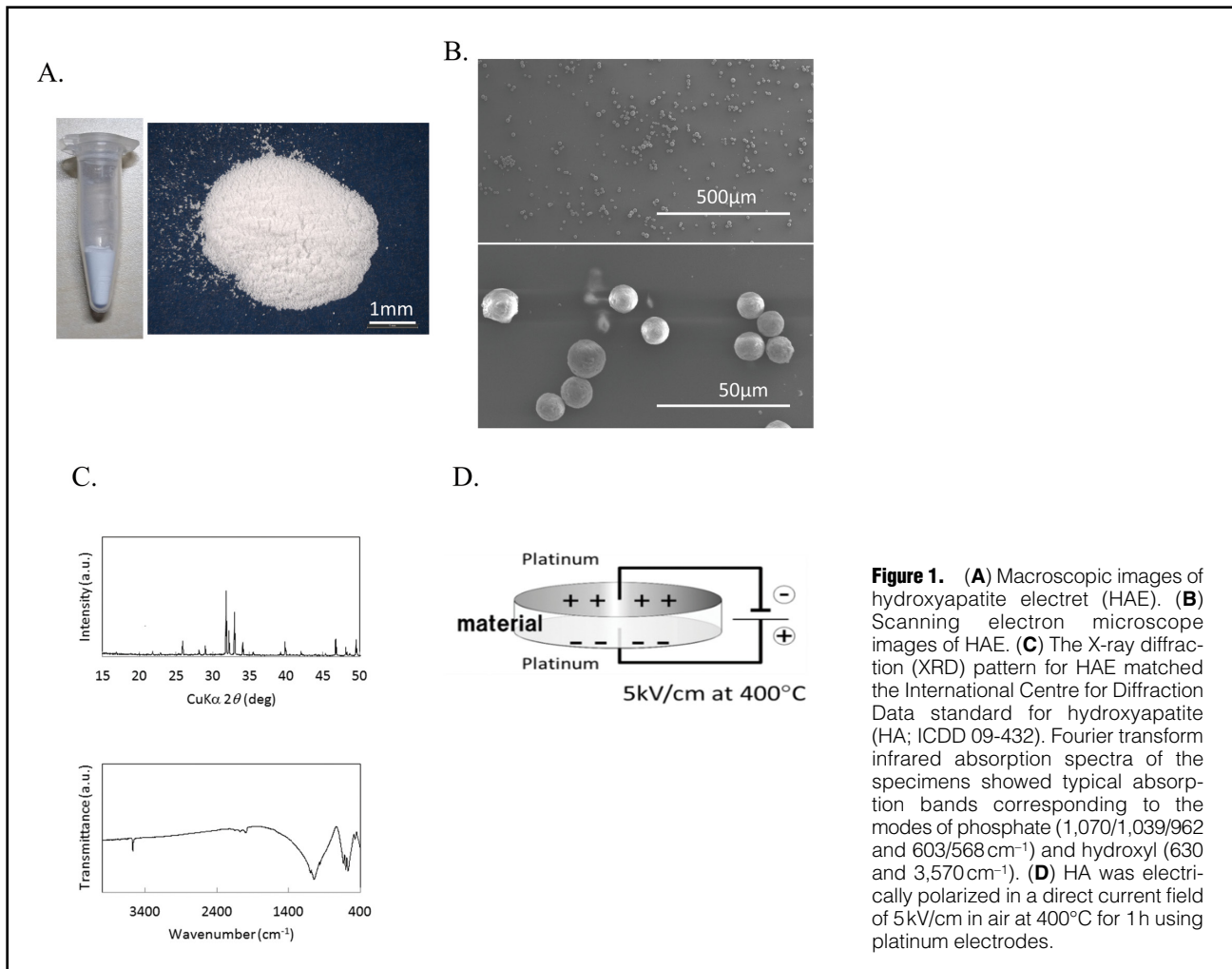


**Figure 1.** (A) Macroscopic images of hydroxyapatite electret (HAE). (B) Scanning electron microscope images of HAE. (C) The X-ray diffraction (XRD) pattern for HAE matched the International Centre for Diffraction Data standard for hydroxyapatite (HA; ICDD 09-432). Fourier transform infrared absorption spectra of the specimens showed typical absorption bands corresponding to the modes of phosphate (1,070/1,039/962 and 603/568  $\text{cm}^{-1}$ ) and hydroxyl (630 and 3,570  $\text{cm}^{-1}$ ). (D) HA was electrically polarized in a direct current field of 5 kV/cm in air at 400°C for 1 h using platinum electrodes.

$\text{K}\alpha$  radiation. The XRD pattern matched the International Centre for Diffraction Data standard for HA (ICDD 09-432; **Figure 1C**). Fourier transform infrared (FTIR) spectra were acquired using the KBr pellet method (FT/IR-4000; JASCO, Tokyo, Japan; **Figure 1C**). FTIR absorption spectra of the specimens showed typical absorption bands corresponding to the modes of phosphate (1,070/1,039/962 and 603/568  $\text{cm}^{-1}$ ) and hydroxyl (630 and 3,570  $\text{cm}^{-1}$ ). After these evaluations, HA was electrically polarized in a direct current (DC) field of 5 kV/cm in air at 400°C for 1 h using platinum electrodes (**Figure 1D**). HAN was prepared using the same method, but without the polarization. The electrical properties of HAE were evaluated by measuring the thermally stimulated depolarization current (TSDC; Keithley Inc., Solon, OH, USA).<sup>7</sup> The maximum current density and mean stored electrical charges of HAE were 1.1 nA/cm<sup>2</sup> and 919 nC/cm<sup>2</sup>, respectively. Conversely, TSDC was not detected in HAN. HAE and HAN were prepared as suspensions in water (1 mg/mL).

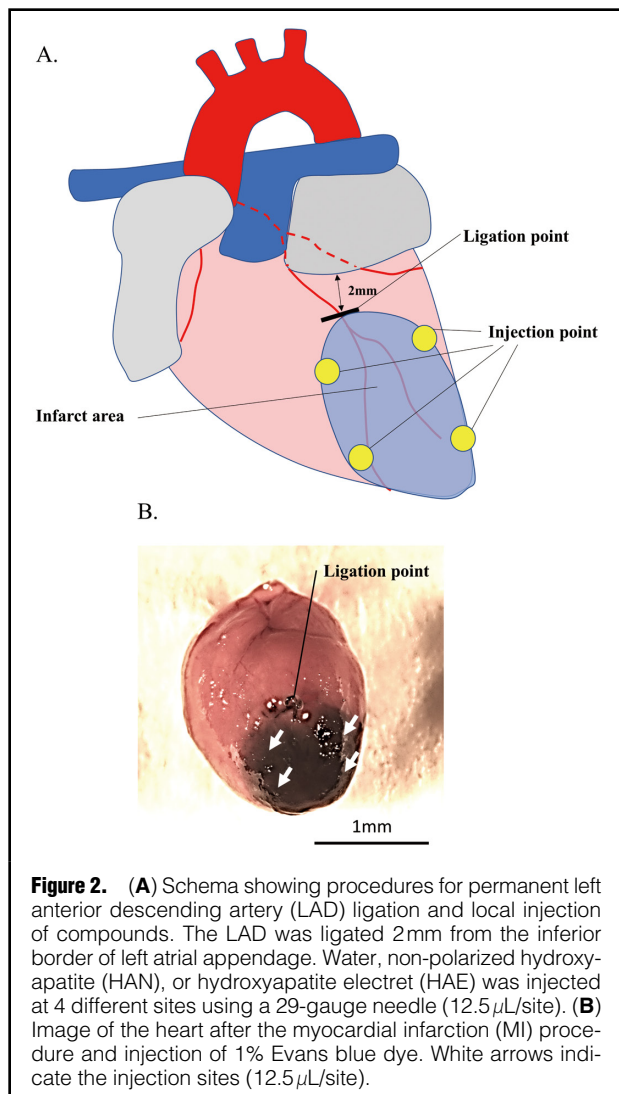
### MI Model

All animal experiments were performed in accordance with the guidelines for the Care and Use of Laboratory Animals published by National Research Council (The National Academy Presses, 8th edition, 2011) and were approved by the Institutional Animal Care and Use

Committee of Tokyo Medical and Dental University (Approval #A2021-014C2).

Anterior MI was induced in male C57BL/6J mice aged 10–12 weeks by permanent ligation of the left anterior descending artery (LAD) as follows. Mice were anesthetized with 1–2% isoflurane under mechanical ventilation (Minivent, Model 845; Harvard Apparatus, Holliston, MS, USA). Then, the pectoral muscles were dissected, the left thorax was opened at the fourth intercostal space, and the LAD was ligated with an 8–0 silk suture.

Immediately after ligation of the LAD, HAE or HAN suspensions were directly injected into the border zone between the infarct and the border myocardium. Distilled water was injected as a control. Local injections were performed at 4 different sites (proximal medial, proximal lateral, distal medial, and distal lateral site) using a 29-gauge needle (**Figure 2**), with a volume of 12.5  $\mu\text{L}$  per injection site. After injection, the intercostal space was closed with 5–0 silk. The skin was also sutured with 5–0 silk. After confirmation of spontaneous breathing, mice were put onto a heated pad and allowed to recover fully. The schema of LAD ligation and local injections is shown in **Figure 2A**. To confirm the area covered by the HAN and HAE suspensions, the same volume of 1% Evans blue dye was injected after LAD ligation, which almost fully covered infarct border zone (**Figure 2B**).



**Treatment With an Anti-VEGF Receptor 2 Blocking Antibody**  
 HAE injected-mice were given intraperitoneal injections of anti-VEGF receptor 2 (VEGFR2) blocking antibody (DC101; BioXcell; 40 mg/kg in phosphate-buffered saline [PBS]) or the corresponding isotype-matched control antibody (IgG1; BioXcell; 40 mg/kg in PBS). Control mice injected with distilled water were given intraperitoneal injections of the control antibody. Injections started 1 h after the MI procedure (Day 0) and were repeated twice a week (i.e., on Days 3, 7, and 10).

### Ultrasound Echocardiography

Two weeks after the surgery, cardiac function was assessed by transthoracic echocardiography (Vevo 770; FUJIFILM Visualsonics, Toronto, Canada). From the short-axis image of the left ventricle (LV), LV end-diastolic diameter (LVDd), LV anterior wall thickness, and LV ejection fraction (LVEF) were measured and calculated.

### Telemetry

A telemetry device (Data Sciences International, St Paul, MN, USA) was implanted 2 days or more ahead of the MI procedure. Mice were anesthetized with 1–2% isoflurane

and the telemetry devices were implanted on their back. Recordings were made 2 h after the surgery for 3–6 h between 09:00 and 15:00 hours.

Electrocardiogram (ECG) signals were recorded using a telemetry receiver (Data Sciences International) and were digitally band-pass filtered (4–140 Hz) using a data acquisition system (PowerLab; ADInstruments, Sydney, NSW, Australia). Time and frequency domain analyses were performed using dedicated software (LabChart 7; ADInstruments). For standardization, only stable segments of sinus rhythm were used for analysis. Heart rate (HR) and HR variability parameters (i.e., standard deviation of NN intervals [SDNN], root mean square of successive differences [RMSSD], low-frequency [LF] range, high-frequency [HF] range, and LF/HF) were assessed among the 3 groups. Cut-off frequencies for power in the LF and HF ranges were based on previous studies.<sup>9,10</sup> ECG periods lasting 120 s without erratic fluctuations were selected in every 60-min period.

### Histological Assessment

After echocardiography, the hearts were harvested, washed, and fixed in 10% formalin for 2 days. Hearts were embedded in paraffin, and paraffin sections were sliced in short-axis sections, followed by Masson's trichrome staining. Samples were photographed at the mid-papillary level using a BZ-X710 microscope (Keyence, Osaka, Japan). The LV was divided into scar area and remote unaffected area. The edge of the scar area was defined by lines that connected the endocardial and epicardial scar borders. For the outer border, the edge was defined as the border between red and blue colors. For the inner border, after excluding the thin layer of viable myocardium (which existed in all cases) and papillary muscles, the edge was defined as the same way as that of the outer border. Schema and representative case are shown in **Supplementary Figure 1**. After drawing the outer circumferential trace of the LV, the length of the scar was calculated as a ratio to the whole LV. The thickness of the scar area was measured at the thinnest portion in the scar region. The viable myocardial area in the scar region and the fibrotic area in the remote region were calculated. These parameters were quantified using ImageJ software (National Institutes of Health [NIH], Bethesda, MD, USA).

For immunohistochemistry, hearts were harvested, washed in PBS, and then fixed in 4% paraformaldehyde (PFA) overnight at room temperature. The PFA was then exchanged for 70% ethanol and the samples were embedded in paraffin and then sectioned (4  $\mu$ m). The paraffin sections were deparaffinized, followed by antigen retrieval using boiling citrate buffer for 40 min. Samples were then blocked with Block Ace powder (KAC, Kyoto, Japan). The sections were incubated for 1 h with antibodies against CD31 (1 : 50 dilution; ab28364; abcam, Cambridge, UK). Sections were examined and photographed using a BZ-X710 microscope (Keyence). The percentage of CD31-positive cells was quantified using ImageJ software (NIH).

### RNA Extraction From LV Tissue and Reverse Transcription

RNA was extracted from 10–30 mg LV tissue using an RNeasy mini kit (Qiagen, Hilden, Germany) according to manufacturer's instructions with an additional purification step by on-column DNase treatment to ensure elimination of any genomic DNA. The quantity of RNA was determined using a NanoDrop 1000 spectrophotometer (Thermo Fisher Scientific, Waltham, MA, USA). cDNA was synthesized

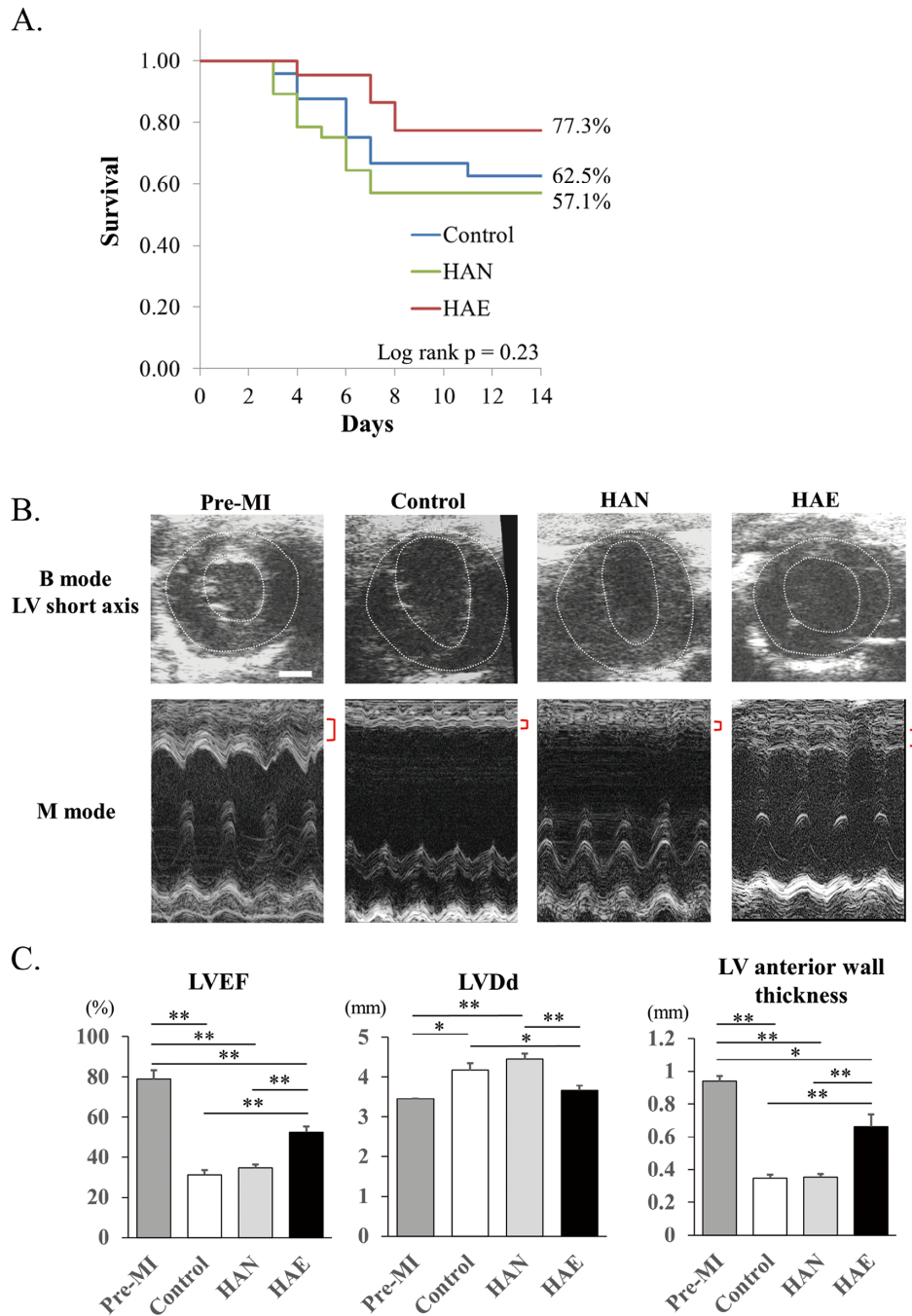


**Figure 3.** (A) Kaplan-Meier survival curves after myocardial infarction (MI) and local injection of water (control), non-polarized hydroxyapatite (HAN), or hydroxyapatite electret (HAE;  $n=22-28$  per group). The log-rank test was used to compare survival distributions among the 3 groups. (B) Representative echocardiographic images of the left ventricle (LV) short axis in end-diastole 2 weeks after the operation. Red brackets indicate the LV anterior wall. Scale bar, 1 mm. (C) Echocardiographic results 2 weeks after the operation ( $n=8$  per group). LVEF, LV ejection fraction; LVDD, LV end-diastolic diameter. Data are the mean  $\pm$  SD. \* $P<0.05$ , \*\* $P<0.01$  (1-way ANOVA followed by Tukey's multiple comparison test).

using a High Capacity cDNA Reverse Transcription Kit (Thermo Fisher Scientific) according to the manufacturer's instructions.

**Endothelial Cell Culture and Experiments**

The human cardiovascular endothelial cell line EAhy926

was purchased from American Type Culture Collection (Bethesda, MD, USA; ATCC®CRL-2922™). EAhy926 cells were cultured in Dulbecco's modified Eagle's medium (DMEM) with 10% fetal bovine serum and 100 U/mL penicillin-streptomycin.

EAhy926 cells were seeded in 96-well cell culture plates

Table. HR and HR Variability in the 3 Groups				
	Control	HAN	HAE	P value
Mean HR (beats/min)	600±64	581±50	609±58	0.275
Mean RR interval (ms)	101±10	104±9	100±11	0.339
SDNN (ms)	6.9 [4.1–16.1]	8.6 [3.3–20.4]	9.0 [3.9–15.9]	0.939
RMSSD	8.4 [5.2–22.0]	11.4 [4.2–26.3]	10.0 [5.0–20.6]	0.996
LF (ms <sup>2</sup> )	10.1 [3.2–53.2]	10.8 [1.1–100.0]	26.0 [0.8–72.8]	0.94
HF (ms <sup>2</sup> )	27.1 [6.7–129.4]	29.7 [4.2–215.7]	33.6 [5.0–173.4]	0.992
LF/HF	0.40±0.16	0.36±0.18	0.40±0.30	0.807

Mice were injected with water (control), non-polarized hydroxyapatite (HAN), or hydroxyapatite electret (HAE) after the induction of myocardial infarction. There were 6 mice in each group and 19–22 (120-s) sections were evaluated in each group. Normally distributed variables were compared among 3 groups using 1-way analysis of variance (ANOVA); non-normally distributed variables were compared using the Kruskal-Wallis test. Unless indicated otherwise, data are presented as the mean±SD or as the median [interquartile range]. HF, high-frequency range (1.5–5 Hz); HR, heart rate; LF, low-frequency range (0.4–1.5 Hz); RMSSD, root mean square of successive differences; SDNN, standard deviation of NN intervals.

at a density of  $2.5 \times 10^6$  cells/well and incubated for 24 h. Distilled water, HAN, and HAE suspensions were added to each well. Three doses of HAN and HAE were tested: 0.1 mg (1 mg/mL), 0.3 mg (3 mg/mL), and 1 mg (10 mg/mL).

Expression of vascular endothelial growth factor (*Vegf*), intercellular adhesion molecule-1 (*Icam1*), vascular cell adhesion molecule-1 (*Vcam1*), hypoxia-inducible factor-1 $\alpha$  (*Hif1a*), and C-X-C motif chemokine ligand 12 (*Cxcl12*) genes was examined by quantitative polymerase chain reaction (qPCR) after 2 days exposure of cells to HAN, HAE, or distilled water. Cell lysis and reverse transcription were performed using a SuperPrep II Cell Lysis RT Kit for qPCR (TOYOBO) according to the manufacturer's instructions.

### Quantitative Reverse Transcription-PCR

Quantitative reverse transcription-PCR analysis was performed using a Step One Plus Real-Time PCR System with Power SYBR Green PCR Master Mix (Thermo Fisher Scientific). Mouse and human glyceraldehyde-3-phosphate dehydrogenase (*mGapdh* and *hGAPDH*, respectively) were used as housekeeping genes. Primer sequences are provided in the **Supplementary Table**.

### Statistical Analysis

Data for normally distributed variables are presented as the mean±SD, whereas data for variables that were not normally distributed are presented as the median and interquartile range. For normally distributed variables, 1-way analysis of variance (ANOVA) was used to compare 3 or more groups, followed by Tukey's multiple comparison test. For non-normally distributed variables, the Kruskal-Wallis test was used, followed by Bonferroni's multiple comparison test. Two-way ANOVA was used to check how 2 independent variables, in combination, affected a quantitative variable. All statistical analyses were performed using R software (R Foundation for Statistical Computing, Vienna, Austria).

## Results

### Effects of HAE on Cardiac Function After MI

Kaplan-Meier analysis was used to evaluate the effects of HA injection on survival after MI (**Figure 3A**). Survival rates 14 days after MI were 62.5%, 57.1%, and 77.3% in the control, HAN, and HAE groups, respectively (log-rank

$P=0.23$ ). Although there was a high probability that HAE-injected mice would survive after MI, there was no significant difference among the 3 groups.

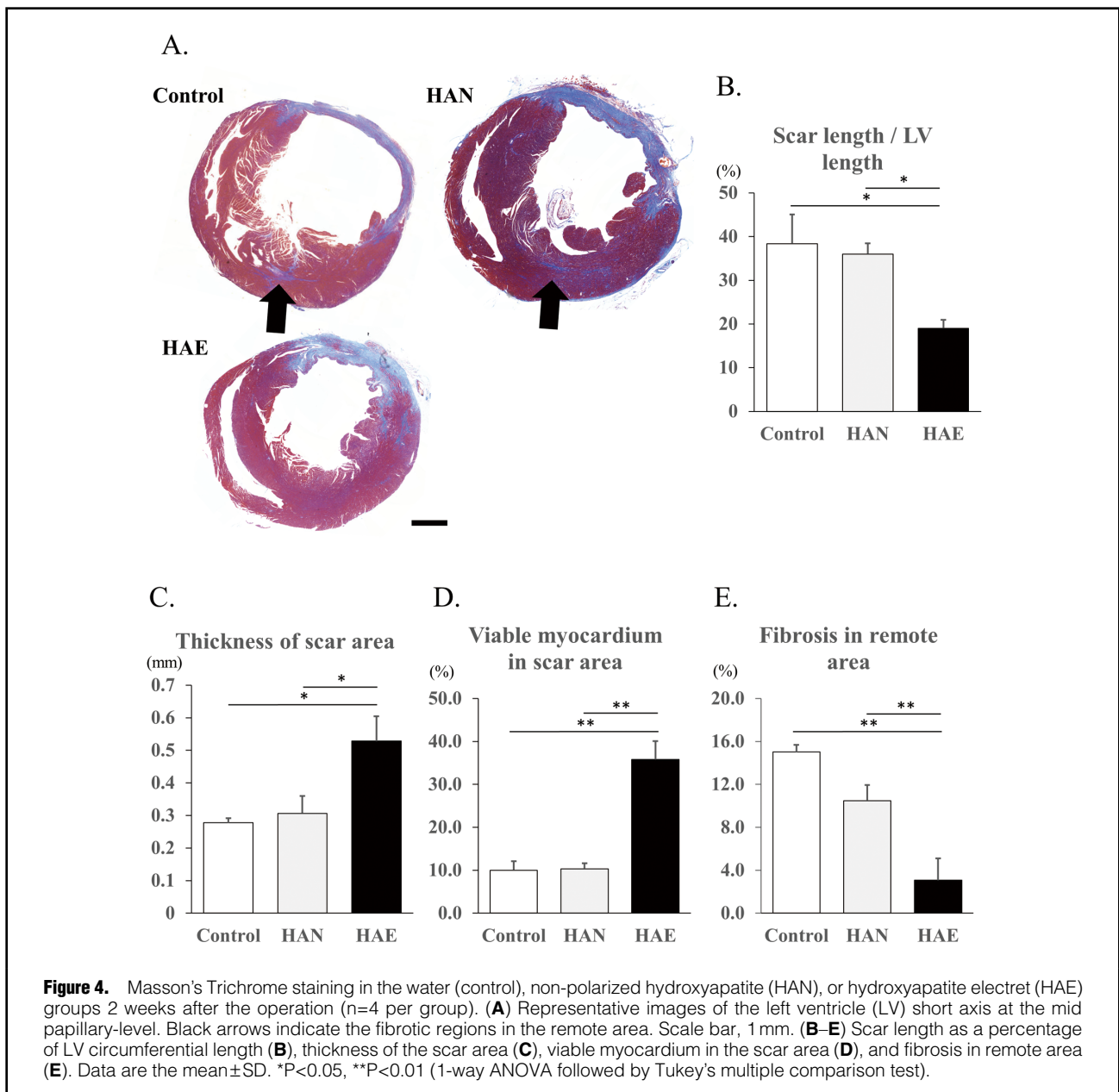
To test whether injection of HAE improved cardiac function after MI, echocardiography was performed 2 weeks after the operation (**Figure 3B,C**). LVEF was significantly higher in the HAE group than in the HAN or control groups (52.5±2.7% vs. 34.6±1.6% and 31.4±2.2%, respectively;  $P<0.001$ , ANOVA). Reflecting the preserved LVEF, LVDD was significantly smaller in the HAE group than in the HAN and control groups (3.66±0.13 vs. 4.45±0.13 and 4.18±0.17 mm, respectively;  $P=0.003$ , ANOVA). Furthermore, LV anterior wall thickness was significantly larger in the HAE group than in the HAN and control groups (0.66±0.08 vs. 0.35±0.02 and 0.35±0.02 mm, respectively;  $P<0.001$ , ANOVA). Tukey's multiple comparison test revealed that the HAE group differed significantly from the control and HAN groups, but there were no significant differences between the HAN and control groups for all measurements. LVEF, LVDD, and LV anterior wall thickness differed significantly from before to after MI in the control, HAN, and HAE groups, with the exception of LVDD in the HAE group.

### Effects of HAE on HR Variability

To check for direct effects of HAE on the vagal nerve, telemetry recordings were performed after MI and local injections. There were no significant differences in HR, SDNN, RMSSD, LF, HF, or LF/HF between the 3 groups (**Table**).

### Effects of HAE on Infarct Scar

We next evaluated the infarct scar by histological assessment. Masson's trichrome staining revealed that the HAE-injected group had a shorter infarct scar length, preserved thickness of the scar region, and a greater area of viable myocardium inside the scar region (**Figure 4A**). Moreover, a fibrotic region was found in the remote area in the control and HAN groups, especially at the right ventricular insertion point (**Figure 4A**). However, this fibrotic infiltration was not observed in the HAE group. Scar length as a percentage of LV circumferential length was significantly lower (**Figure 4B**) and the thickness of the scar area was significantly larger in HAE-injected mice (**Figure 4C**). The ratio of viable myocardium in the scar region was significantly larger, but the fibrotic area in the remote region was



significantly smaller in HAE-injected mice (**Figure 4D,E**). These findings indicate that HAE injection reduced the infarct scar and attenuated ventricular remodeling after MI. Of note, the histological assessment did not detect HAE or HAN particles in the myocardium. Because these HA particles are bioabsorptive materials, they were absorbed within 2 weeks.

#### Effects of HAE on Angiogenesis in the Infarct Border Zone

The preceding experiments confirmed the effects of HAE in preserving cardiac function and attenuating LV remodeling. We investigated the mechanism underlying the favorable effects of local injections of HAE, focusing on angiogenesis. Immunohistochemistry revealed that infiltration of CD31, a marker of endothelial cells was significantly increased in the HAE group compared with the HAN and control

groups ( $3.85 \pm 0.19\%$  vs.  $1.85 \pm 0.14\%$  and  $1.68 \pm 0.18\%$ , respectively;  $P < 0.001$ ; **Figure 5**).

In addition, the expression of *Vegf*, *Icam1*, *Vcam1*, *Hif1a*, and *Cxcl12* in the border zone myocardium was examined by qPCR (**Figure 6**). *Vegf* expression was significantly increased in the HAE group compared with the HAN and control groups. Expression of *Icam1*, *Vcam1*, and *Cxcl12* was also significantly higher in the HAE group than in the other 2 groups. *Hif1a* expression was significantly higher in the HAE group compared with control group ( $P = 0.04$ ), but did not differ significantly between the HAE and HAN groups ( $P = 0.08$ ).

#### Anti-VEGFR2 Antibody on the Effects of HAE

An anti-VEGFR2 blocking antibody (DC101) was used to confirm that the mechanism by which HAE improved

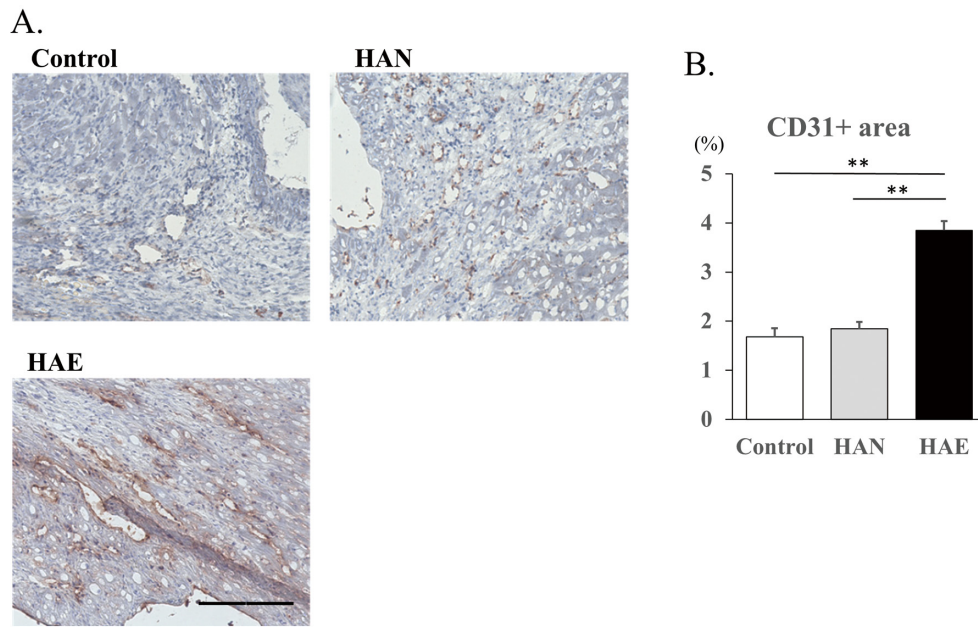


**Figure 5.** (A) Representative images of immunohistochemistry for vascular endothelial cells using an anti-CD31 antibody in the infarct border zone myocardium in the water (control), non-polarized hydroxyapatite (HAN), or hydroxyapatite electret (HAE) groups. Scale bar, 100 $\mu$ m. (B) The percentage of CD31-positive cells in each of the groups. Data are the mean $\pm$ SD (n=4 per group). \*\*P<0.01 (1-way ANOVA followed by Tukey's multiple comparison test).

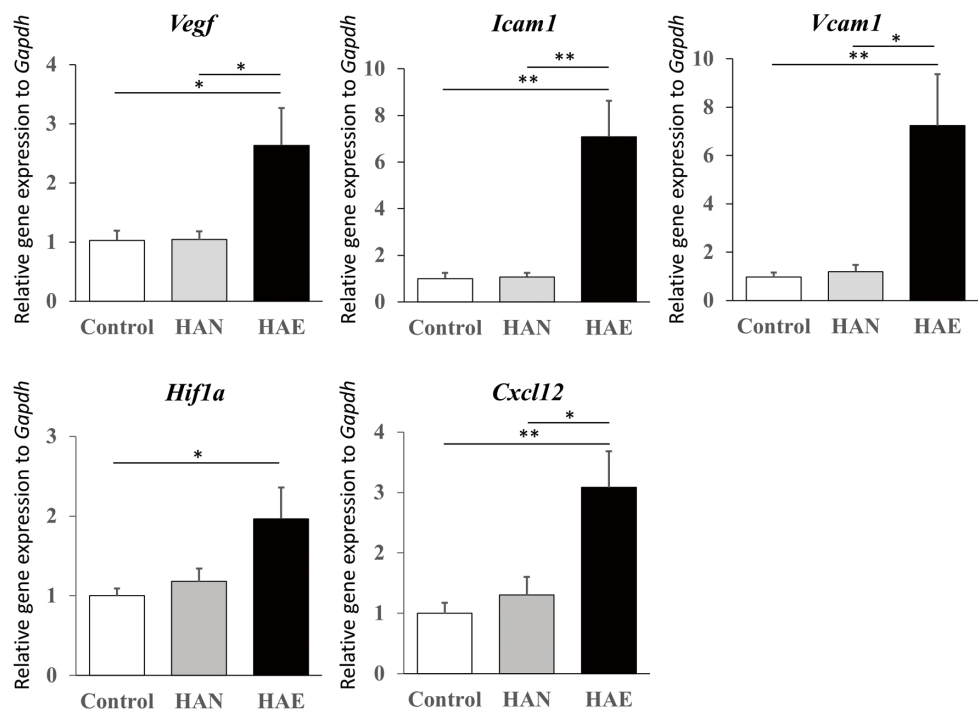
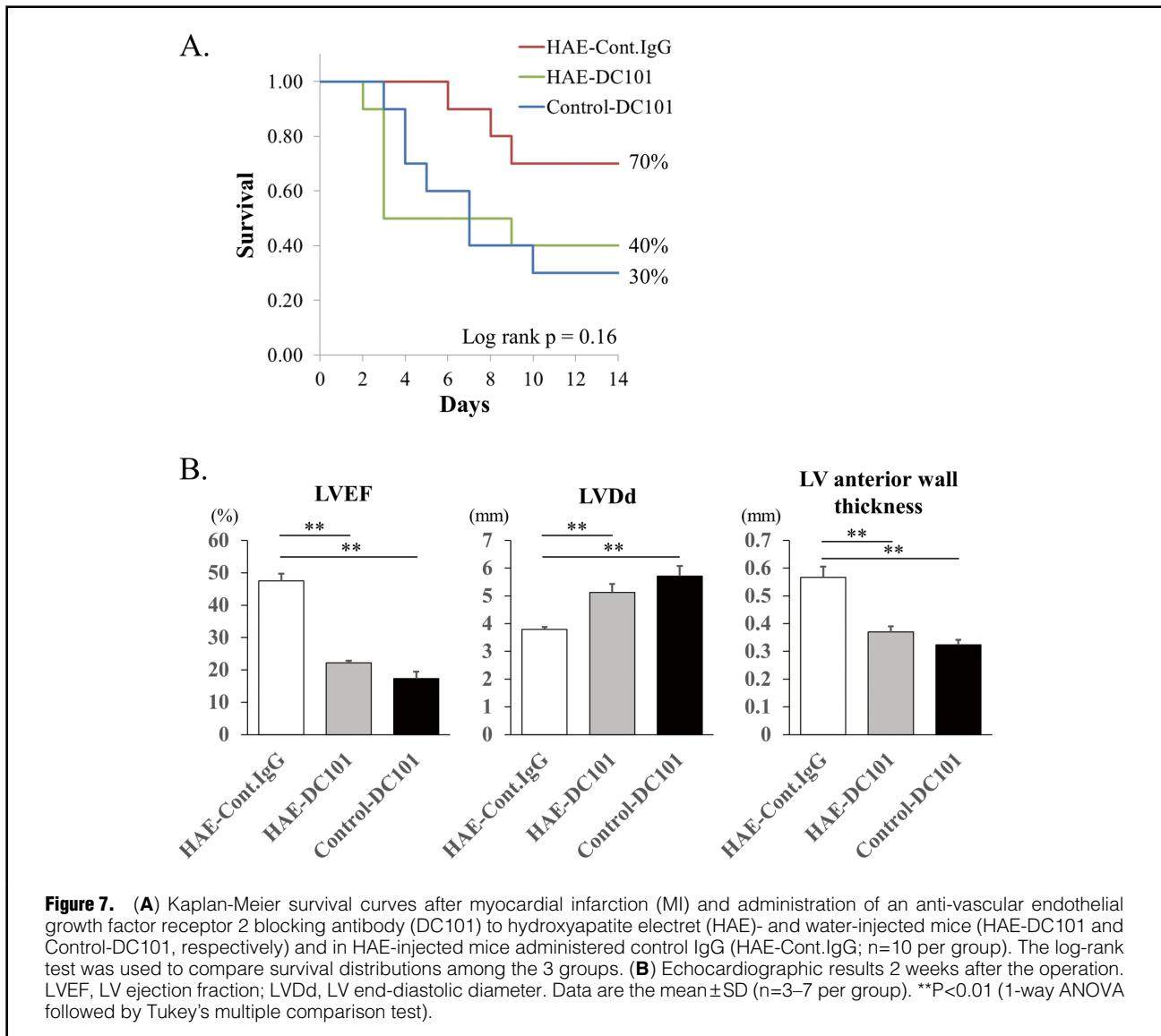


**Figure 6.** Relative expression of vascular endothelial growth factor (*Vegf*), intercellular adhesion molecule-1 (*Icam1*), vascular cell adhesion molecule-1 (*Vcam1*), hypoxia-inducible factor-1 $\alpha$  (*Hif1a*), and C-X-C motif chemokine ligand 12 (*Cxcl12*) in the infarct border zone myocardium. Data are the mean $\pm$ SD (n=5–7 per group). \*P<0.05, \*\*P<0.01 (1-way ANOVA followed by Tukey's multiple comparison test).



cardiac function and ameliorated infarct size in mice was via the VEGF pathway. Survival rates in HAE- and water-injected mice administered DC101 (HAE-DC101 and Control-DC101, respectively) were similarly low (40% and 30%, respectively; **Figure 7A**). However, the survival rate in HAE-injected mice administered control IgG (HAE-Cont.IgG) was 70%, which is similar to the survival rate of HAE-injected mice without control IgG (77.3%).

Echocardiographic results are shown in **Figure 7B**. LVEF was significantly lower in the HAE-DC101 and Control-DC101 groups than in the HAE-Cont.IgG group ( $22.2 \pm 0.6$  and  $17.3 \pm 2.1$  vs.  $47.5 \pm 2.3\%$ , respectively;  $P < 0.001$ , ANOVA). LVDD was significantly greater in the HAE-DC101 and Control-DC101 groups than in the HAE-Cont.IgG group ( $5.13 \pm 0.30$  and  $5.71 \pm 0.37$  vs.  $3.80 \pm 0.08$  mm, respectively;  $P < 0.001$ , ANOVA). Furthermore, LV anterior wall thickness was smaller in the HAE-DC101 and Control-DC101 groups than in the HAE-Cont.IgG group ( $0.37 \pm 0.02$  and  $0.32 \pm 0.02$  vs.  $0.57 \pm 0.04$  mm, respectively;  $P = 0.001$ , ANOVA). Tukey's multiple comparison test

revealed significant differences between the HAE-Cont.IgG group and both the HAE-DC101 and Control-DC101 groups, but no significant differences between the HAE-DC101 and Control-DC101 groups.

#### Effects of HAE on VEGFA Expression in Human Endothelial Cells

To confirm the effect of HAE in vitro, *VEGFA* expression in EAhy926 cells was examined by qPCR (**Supplementary Figure 2**). HAE dose-dependently increased *VEGFA* expression. At a concentration of 10 mg/mL, HAE increased *VEGFA* expression to a significantly greater extent than 10 mg/mL HAN ( $P = 0.046$ , Tukey's multiple comparison test). Two-way ANOVA was used to check the effects of concentration (1, 3, and 10 mg/mL) and compound (HAN and HAE) on *VEGFA* expression levels. The results showed significant differences in *VEGFA* expression depending on the concentration used ( $F_{2,26} = 22.6$ ,  $P < 0.001$ ), as well as the compound used ( $F_{1,26} = 7.7$ ,  $P < 0.001$ ). The  $P$  value for the interaction of these terms was not significant ( $P = 0.25$ ).

Further examination of the effect of concentration used Tukey's multiple comparison test revealed significant differences among groups (1 vs. 3mg/mL,  $P=0.049$ ; 1 vs. 10mg/mL,  $P<0.001$ ; 3 vs. 10mg/mL,  $P=0.02$ ). At a concentration of 10mg/mL, HAN and HAE already fully covered the surface of EAhy926 cells; therefore, further effects would not be expected with higher concentrations.

## Discussion

The present study examined the effects of local HAE injections on cardiac function and infarct size after MI. HAE-injected mice had significantly better cardiac function and an ameliorated infarct size based on echocardiography and histology. These effects were accompanied by a higher percentage of vascular endothelial cells and higher expression of *Vegf*, *Icam1*, *Vcam1*, *Hif1a*, and *Cxcl12*. An angiogenic effect through VEGF was shown by the pharmacological inhibition of VEGFR2. An effect of HAE in increasing VEGF was further supported by an in vitro study using human cardiovascular endothelial cells. To the best of our knowledge, this is the first report to demonstrate that HAE significantly ameliorates infarct size after MI. Because these changes were not evident in HAN-injected mice, the effects may be caused by the static electric charge of polarized HA particles.

A previous study demonstrated the effects of HAE on the regeneration of functioning endothelial cells in the rabbit carotid artery, whereby HAE application, but not HAN application, accelerated re-endothelialization and attenuated intimal hyperplasia after removal of the endothelium in the carotid artery.<sup>7</sup> In the present study, we clearly demonstrated that local injection of HAE, but not HAN, induced significant angiogenesis after MI, which appears to be compatible with the previously reported results. The increased angiogenic activity in the present study was evidenced by the increased number of CD31-positive cells and elevated *Vegf* expression in HAE-injected mice compared with control mice. The beneficial effect of enhanced angiogenesis was supported by echocardiography and Masson's trichrome staining. Reflecting angiogenic activity in the infarct border zone, there was a significantly larger area of viable myocardium in the scar area in HAE-injected mice. Moreover, fibrosis in remote unaffected areas, which indicates remodeling of the LV, was significantly smaller and the thickness of scar area was significantly larger in HAE-injected mice.

The angiogenic effect of HAE has also been reported in previous study, in which the analysis was limited to histological findings alone.<sup>6</sup> In the present study, we confirmed the angiogenic effect of HAE not only using histological assessment, but also analyzing gene expression levels of *Vegf*, *Cxcl12*, and *Hif1a*. Considering that the only difference between HAE and HAN is the polarization, it is reasonable to expect that the cardioprotective effect of HAE observed in the present study may be induced by the polarization itself.

In the recent years, it has been reported that electrical stimulation or a pulsed magnetic field (PMF) induces the production of VEGF and induces angiogenesis in vivo.<sup>11,12</sup> Although most studies have investigated the effects of PMF on limb ischemia, studies on myocardial ischemia using PMF are increasingly being reported. For example, Yuan et al reported that 28 days of PMF therapy (3h/day) significantly improved ventricular function and reduced infarct

size by increased angiogenesis via the VEGF/VEGFR2 pathway.<sup>13</sup> Peng et al reported that PMF treatment significantly induced angiogenesis of the infarct border zone via the HIF1 $\alpha$ /VEGF and HIF1 $\alpha$ /fibroblast growth factor 2 signaling pathways.<sup>14</sup> Similar to these reports, significant increases in the expression of *Vegf*, *Cxcl12*, and *Hif1a* were observed in the present study. Endothelial progenitor cells (EPCs) play a vital role in vascular repair through increased mobilization, migration, homing, differentiation, and enhanced neovascularization of ischemic areas.<sup>15</sup> CXCL12, also known as stromal cell-derived factor-1, is a chemokine protein that is crucial for EPC mobilization and homing to ischemic myocardium.<sup>16</sup> *HIF1A* transcription is activated in response to hypoxia, and HIF1 $\alpha$  is known to bind to and directly activate transcription of *VEGF* and *CXCL12*, thus promoting angiogenesis and vascular repair of injured areas.<sup>17</sup> Judging from the elevated expression of these genes in the border myocardium of HAE-injected mice in the present study, the beneficial effects of HAE are likely mediated through the HIF1 $\alpha$ -CXCL12/VEGF signaling pathway. Although HAE has a static electric charge that is different to PMF, HAE likely induces angiogenesis in a similar manner to PMF treatment. There are some advantages of local injections of HAE as therapy. First, unlike PMF therapy, no equipment is required for local injections of HAE. In addition, because the injected HAE is absorbed and disappears from the heart tissue, the risk of long-lasting complications is relatively small.

In the present study, significant elevations in *Icam1* and *Vcam1* were also seen in HAE-injected mice. ICAM1 and VCAM1 are cell adhesion molecules that are predominantly expressed in endothelial cells.<sup>18,19</sup> Wu et al reported that CD18 and its ligand ICAM1 mediate recruitment of bone marrow-derived EPCs, angiogenesis, and repair of the infarcted myocardium.<sup>20</sup> Iwamiya et al reported that local injection of human VCAM1-expressing cardiac fibroblasts in a postinfarct rat model led to a significant restoration of LV contraction by mobilizing lymphatic endothelial cells into the infarct area.<sup>21</sup> These angiogenic and lymphangiogenic effects may also contribute to the beneficial effects of HAE seen in the present study. However, the possibility remains that the increases in *Icam1* and *Vcam1* may simply reflect increases in endothelial cells through the HIF1 $\alpha$ -CXCL12/VEGF signaling pathway.

Results from the in vitro study using EAhy926 cells support our results in vivo. Significant increases of *VEGFA* were seen after application of HAE compared with water and HAN. Moreover, HAE application produced significant, dose-dependent increases in *VEGFA*. In the present in vivo experiment, we used concentrations of 1 mg/mL HAN and HAE for local injections. In preliminary study, we also used a 10-fold higher concentration (10mg/mL) of HAE and HAN, but in with this concentration most of the HAN- and HAE-injected mice died soon after the injection (data not shown). The physical pressure exerted by a large amount of HA may interfere with the contraction of the heart. Additional studies are needed to find the optimal amount to be injected to achieve the maximum effect without complications.

HR variability was assessed in order to check whether the cardioprotective effect of HAE was derived from an effect on the vagal nerve. It has been shown that vagal nerve stimulation has an antifibrillatory effect and leads to improved LV hemodynamics.<sup>22,23</sup> However, in the present study there were no differences in HR variability between

groups; therefore, the polarization of HA did not seem to have a direct effect on the vagal nerve.

One limitation of this study that needs to be noted is that increased angiogenesis may not be the only explanation for the HAE-induced cardioprotective effects. Further studies are needed to investigate the precise mechanisms by which HAE exerts its cardioprotective effects, via VEGF signaling and other potential mechanisms.

## Conclusions

Local injection of HAE in mice was associated with significant preservation of cardiac function and amelioration of infarct size. The HAE-induced benefits were likely due to enhanced angiogenesis via the HIF1 $\alpha$ -CXCL12/VEGF signaling pathway.

## Acknowledgment

The authors thank Noriko Tamura for technical assistance with the histological assessment.

## Sources of Funding

This study was performed with support from The Creation of Life Innovation Materials for Interdisciplinary and International Researcher Development Project, Ministry of Education, Culture, Sports, Science and Technology (MEXT), Japan.

## Disclosures

The authors have no conflicts of interest to declare.

## IRB Information

This study was approved by the Institutional Animal Care and Use Committee of Tokyo Medical and Dental University (Approval #A2021-014C2).

## Data Availability

Data will be shared upon reasonable request to the corresponding author. The data presented in this study, including echocardiography, histological assessment, and qPCR data, will be shared as Excel files. The study protocol and statistical analysis plan will also be shared upon request. The data will be available immediately following publication, ending 10 years after publication.

## References

1. Rentrop KP, Feit F. Reperfusion therapy for acute myocardial infarction: Concepts and controversies from inception to acceptance. *Am Heart J* 2015; **170**: 971–980.
2. Awasthi S, Pandey SK, Arunan E, Srivastava C. A review on hydroxyapatite coatings for the biomedical applications: Experimental and theoretical perspectives. *J Mater Chem B* 2021; **9**: 228–249.
3. Nakamura S, Takada H, Yamashita K. Proton transport polarization and depolarization of hydroxyapatite ceramics. *J Appl Physics* 2001; **89**: 5386–5392.
4. Nakamura M, Sekijima Y, Nakamura S, Kobayashi T, Niwa K, Yamashita K. Role of blood coagulation components as intermediators of high osteoconductivity of electrically polarized hydroxyapatite. *J Biomed Mater Res A* 2006; **79**: 627–634.
5. Nakamura M, Niwa K, Nakamura S, Sekijima Y, Yamashita K. Interaction of a blood coagulation factor on electrically polarized hydroxyapatite surfaces. *J Biomed Mater Res B Appl Biomater*

- 2007; **82**: 29–36.
6. Kobayashi T, Itoh S, Nakamura S, Nakamura M, Shinomiya K, Yamashita K. Enhanced bone bonding of hydroxyapatite-coated titanium implants by electrical polarization. *J Biomed Mater Res A* 2007; **82**: 145–151.
7. Nagai A, Yamashita K, Imamura M, Azuma H. Hydroxyapatite electret accelerates reendothelialization and attenuates intimal hyperplasia occurring after endothelial removal of the rabbit carotid artery. *Life Sci* 2008; **82**: 1162–1168.
8. Nakamura S, Kobayashi T, Yamashita K. Extended bioactivity in the proximity of hydroxyapatite ceramic surfaces induced by polarization charges. *J Biomed Mater Res* 2002; **61**: 593–599.
9. Thireau J, Zhang BL, Poisson D, Babuty D. Heart rate variability in mice: A theoretical and practical guide. *Exp Physiol* 2008; **93**: 83–94.
10. Gehrman J, Hammer PE, Maguire CT, Wakimoto H, Triedman JK, Berul CI. Phenotypic screening for heart rate variability in the mouse. *Am J Physiol Heart Circ Physiol* 2000; **279**: H733–H740.
11. Zhao M, Bai H, Wang E, Forrester JV, McCaig CD. Electrical stimulation directly induces pre-angiogenic responses in vascular endothelial cells by signaling through VEGF receptors. *J Cell Sci* 2004; **117**: 397–405.
12. Chen Y, Ye L, Guan L, Fan P, Liu R, Liu H, et al. Physiological electric field works via the VEGF receptor to stimulate neovessel formation of vascular endothelial cells in a 3D environment. *Biol Open* 2018; **7**: bio035204.
13. Yuan Y, Wei L, Li F, Guo W, Li W, Luan R, et al. Pulsed magnetic field induces angiogenesis and improves cardiac function of surgically induced infarcted myocardium in Sprague-Dawley rats. *Cardiology* 2010; **117**: 57–63.
14. Peng L, Fu C, Liang Z, Zhang Q, Xiong F, Chen L, et al. Pulsed electromagnetic fields increase angiogenesis and improve cardiac function after myocardial ischemia in mice. *Circ J* 2020; **84**: 186–193.
15. Hristov M, Erl W, Weber PC. Endothelial progenitor cells: Mobilization, differentiation, and homing. *Arterioscler Thromb Vasc Biol* 2003; **23**: 1185–1189.
16. Shen L, Gao Y, Qian J, Sun A, Ge J. A novel mechanism for endothelial progenitor cells homing: The SDF-1/CXCR4-Rac pathway may regulate endothelial progenitor cells homing through cellular polarization. *Med Hypotheses* 2011; **76**: 256–258.
17. Rey S, Semenza GL. Hypoxia-inducible factor-1-dependent mechanisms of vascularization and vascular remodeling. *Cardiovasc Res* 2010; **86**: 236–242.
18. Sultan S, Gosling M, Nagase H, Powell JT. Shear stress-induced shedding of soluble intercellular adhesion molecule-1 from saphenous vein endothelium. *FEBS Lett* 2004; **564**: 161–165.
19. Terry RW, Kwee L, Levine JF, Labow MA. Cytokine induction of alternative spliced murine vascular adhesion molecule (VCAM) mRNA encoding a glycosylphosphatidylinositol-anchored VCAM protein. *Proc Natl Acad Sci USA* 1993; **90**: 5919–5923.
20. Wu Y, Ip JE, Huang J, Zhang L, Matsushita K, Liew CC, et al. Essential role of ICAM-1/CD18 in mediating EPC recruitment, angiogenesis, and repair to the infarcted myocardium. *Circ Res* 2006; **99**: 315–322.
21. Iwamiya T, Segard BD, Matsuoka Y, Imamura T. Human cardiac fibroblasts expressing VCAM1 improve heart function in postinfarct heart failure rat models by stimulating lymphangiogenesis. *PLoS One* 2020; **15**: e0237810.
22. Camm AJ, Savelieva I. Vagal nerve stimulation in heart failure. *Eur Heart J* 2015; **36**: 404–406.
23. Schwartz PJ. Vagal stimulation for heart diseases: from animals to men: An example of translational cardiology. *Circ J* 2011; **75**: 20–27.

## Supplementary Files

Please find supplementary file(s);  
<http://dx.doi.org/10.1253/circrep.CR-21-0100>